

Lighting System for Visual Perception Enhancement in Volume Rendering

Lei Wang and Arie E. Kaufman, *Fellow, IEEE*

Abstract—We introduce a lighting system that enhances the visual cues in a rendered image for the perception of 3D volumetric objects. We divide the lighting effects into global and local effects, and deploy three types of directional lights: the key light and accessory lights (fill and detail lights). The key light provides both lighting effects and carries the visual cues for the perception of local and global shapes and depth. The cues for local shapes are conveyed by gradient; those for global shapes are carried by shadows; and those for depth are provided by shadows and translucent objects. Fill lights produce global effects to increase the perceptibility. Detail lights generate local effects to improve the cues for local shapes. Our method quantifies the perception and uses an exhaustive search to set the lights. It configures accessory lights with the consideration of preserving the global impression conveyed by the key light. It ensures the feeling of smooth light movements in animations. With simplification, it achieves interactive frame rates and produces results that are visually indistinguishable from results using the nonsimplified algorithm. The major contributions of this paper are our lighting system, perception measurement and lighting design algorithm with our indistinguishable simplification.

Index Terms—Lighting design, volume rendering, light placement, spherical coordinate system

1 INTRODUCTION

LIGHTING models for direct volume rendering have continued to improve in recent years. Local shading models, such as the Phong model, are suitable to convey visual cues for local shape perception of well-defined structures. Approximations of global illumination, such as the occlusion model [38], provide cues for depth perception. However, the lighting design for volume data visualization remains a challenge.

Lighting design has long been considered crucial in conveying visual cues for the perception of 3D objects [7]. Carelessly configured lights have unintended side effects: shadows hide details with low luminance (the region around the right eye in Fig. 1b); overillumination reduces depth cues and makes objects look flat (Fig. 1c) and even conveys an inconsistent global impression that ruins the cues for global shapes (Fig. 1d). These side effects are worse in visualization applications such as medical applications, where the details and shapes of tissues are expected to be distinguishable. However, previous lighting design methods are not suitable for these applications. The previous approaches for surface rendering [37] ignore the influence of translucent structures on the visibility of surfaces and hence fail to configure lights for volumetric data. The methods using spatially varying lights [24] to produce a globally inconsistent result that conveys a confusing global impression. The curvature-based algorithms [10] emphasize curvature-based features instead of shapes.

In this paper, we propose a lighting system that uses directional lights to enhance the visual cues for the

perception of 3D objects. The lighting system is configured by our lighting design algorithm, which maximizes the perception, including shape perception and depth perception. The visual cues for the local shape perception are carried by diffuse reflection (discussed in Section 3). The local shape perception is computed using gradient magnitude (7). The cues for the global shape perception are conveyed by shadows, and that for the depth perception is provided by shadows and aerial perspective (Section 3). Their corresponding perception is measured using the weighted Pearson correlation coefficient (Section 4.1). Our algorithm considers the influence of translucent layers on the visibility of each voxel. It diminishes the influence of curvature-based features by assuming uniformly distributed curvatures in the measurement of the local shape perception. It also solves the side effects of overillumination and shadows. The major contributions of our work are the perception enhancing lighting system, the quantitative perception measurements, and the automatic lighting design algorithm. Our approach works in spherical coordinates and ensures C1 continuous key light movements in predefined animations. It achieves interactive frame rates on a modern GPU after a visually indistinguishable simplification.

This paper is organized as follows. Section 2 presents previous work and its relationship to ours. Section 3 introduces our lighting system. Section 4 describes the quantitative perception measurements and our lighting design algorithm. The simplification and implementation details are described in Section 5. Section 6 evaluates the direct volume rendering results and the performance of our method, and compares them with the results of other methods. Finally, conclusions and limitations are discussed in Section 7.

2 PREVIOUS WORK

Numerous papers focus on lighting model design, such as diffuse shading [25], ambient occlusion [44], and the

• The authors are with the Department of Computer Science, Stony Brook University (SUNY), Stony Brook, NY 11794-4400.
E-mail: {leiwang1, xinzha, ari}@cs.stonybrook.edu.

Manuscript received 25 Aug. 2011; revised 22 Jan. 2012; accepted 23 Feb. 2012; published online 13 Mar. 2012.

Recommended for acceptance by R. Machiraju.

For information on obtaining reprints of this article, please send e-mail to: tvcg@computer.org, and reference IEEECS Log Number TVCG-2011-08-0199. Digital Object Identifier no. 10.1109/TVCG.2012.91.

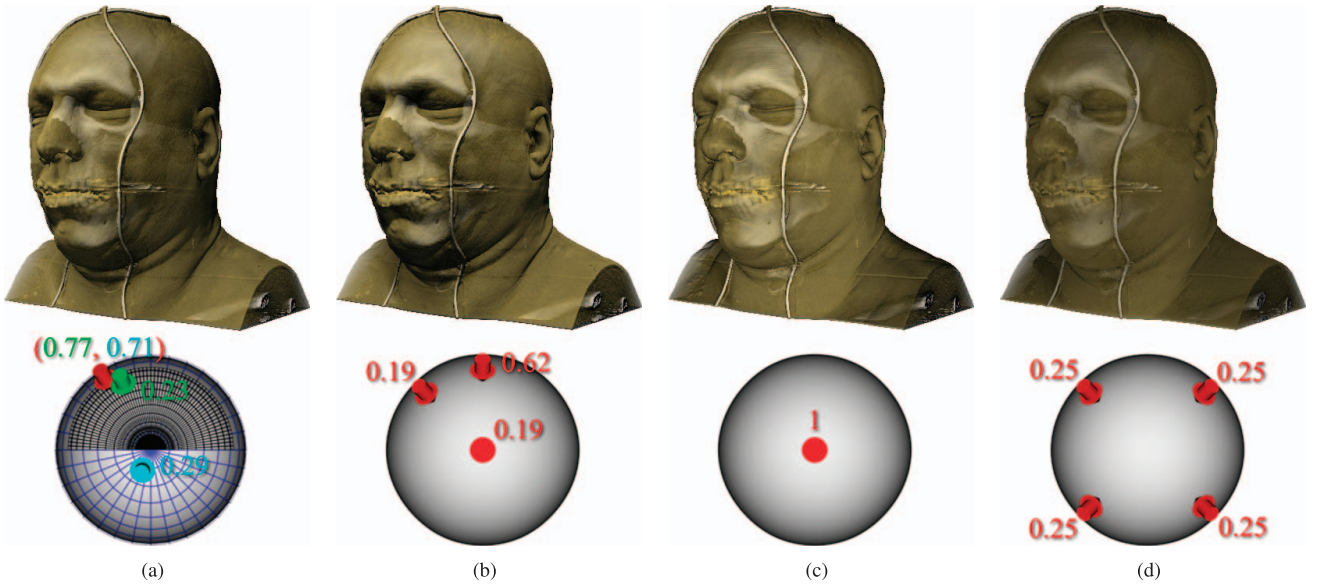


Fig. 1. Direct volume rendering of the Visible Man's head with different light configurations: (a) our method, (b) butterfly lighting method, (c) single headlight, and (d) four consistent lights. The directions of the lights are shown as 3D arrows (the arrow showing the view direction is displayed as a dot). The numbers indicate the corresponding intensities with colors representing the lighting effects: green is global effects, light blue is local effects, and red refers to both effects. The black and blue 3D grids in (a) display the search spaces of the key light and accessory lights, respectively.

occlusion shading model [38]. Meanwhile, the importance of lighting design for determining the appearance of the resulting scene has been discussed in detail in the field of photography [1], [26], cinematography [4] and stage lighting [29]. These classic techniques have been summarized by Apodaca and Gritz [21] and Kahrs et al. [20] for computer-generated imagery.

Some of the former lighting design methods are direct, where the user directly specifies the lighting parameters. In these methods, the user starts out by setting an initial light configuration and visually evaluates the result to modify the lighting parameters. Marks et al. [28] have asked the user to hierarchically select the rendering images that are generated using user-specified parameters with random light positions. Halle and Meng [17] have provided the LightKit system to allow the user to interactively adjust the lighting parameters. These direct methods are time consuming and require significant expertise in lighting design. In contrast, our system automatically configures the lights.

Many current lighting design methods are classified as indirect lighting methods. In these methods, the user specifies the desired highlights or shadows and the system then infers the lighting configuration to achieve them [18], [32]. In a subfield of indirect lighting design, which is called procedural indirect lighting design, the system automatically configures the lighting parameters by optimizing a set of criteria based on the given scene. Gumhold [16] has developed a light placement strategy by using the perceptual entropy of the rendered image as the criterion. Entropy is a measure of how many structures are displayed, but not how well they are revealed. Our approach maximizes how well the structures are conveyed. The method proposed by Chan et al. [10] uses accumulated curvature, but ignores the influence of translucent layers. Shacked and Lischinski's algorithm [37] works by placing up to two lights by maximizing a perception-based objective function that contains a shape derivation for surface rendering. However,

their shape derivation is highly affected by curvatures. These curvature-based methods inevitably emphasize curvature-based features and overlook local shapes. In contrast, our work diminishes the side effect of curvature-based features and considers the influence of translucent structures.

Methods using spatially varying lights have been proposed by researchers. Lee et al. [24] have discussed the idea of using multiple lights to locally illuminate different regions for geometry-dependent lighting design. Nevertheless, the global impression cannot be guaranteed in their results and shadows are added as supplementary features without optimization. Our method preserves the global impression and maximizes the perception from shadows. Rusinkiewicz et al. [35] have investigated cartographic terrain relief to dynamically adjust the effective light position for different areas of a surface. Their approach preserves the global impression by using multiscale processing. However, the human visual system perceives the local and global perception in different ways and hence their method fails to simultaneously guarantee the local and global perception. In contrast, our approach measures the local and global perception separately based on the human visual system and it maximizes them in the same image.

Other efforts using nonphotorealistic rendering have also been done. Gooch et al. [15] have developed a lighting model that uses luminance and changes in hue to convey surface orientation, edges, and highlights. Sousa et al. [39] have incorporated lighting into stroke lengths. Vergne et al. [40] have warped the light and have modified the radiance scaling [41]. On the contrary, we enhance the visual cues of photorealistic rendering. Bousseau et al. [6] have optimized environment maps to depict material. Bergner et al. [8] have implemented spectral volume rendering to reveal different objects. Compared with these methods, our method focuses on the enhancement of visual cues for shape and depth perception.

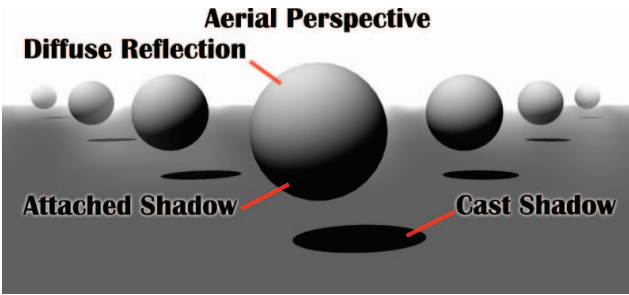


Fig. 2. Rendering of spheres in a cloud showing the major lighting effects: local effects (diffuse reflection and attached shadow) and global effects (cast shadow and aerial perspective).

3 LIGHTING SYSTEM

Our first contribution is the lighting system that enhances visual cues for the shape and depth perception. A lighting system should contain a key light, fill light and back light [20], [21]. The key light is the primary source of illumination and visual cues. It conveys the global impression of a scene. The fill light softens and fills the shadows. It mainly increases the perceptibility of a scene. The back light separates the object from the background. Our lighting system changes the back light to detail light because of the absence of a background in most volumetric data, whereas the detail light is implied to emphasize local shapes.

Our lighting system uses directional lights. Considering a light ray hitting a voxel, the intensity of the incident light (called *illuminance*) is computed using a multidirectional occlusion model [38] and the brightness of the reflected light (called *luminance*) is calculated based on the Phong shading model. The reflected light, then, travels through the translucent objects and arrives at the viewpoint to form an image. The contribution of a reflected light to its corresponding pixel in the rendered image is termed *perceived luminance*.

The lighting effects that are primarily considered as the sources of visual cues are shown in Fig. 2. Diffuse reflection is the primary source of cues for local shape perception [19]. A cast shadow informs about the global shape, depth information and spatial arrangement of the objects [27]. Together with an attached shadow, it supports the visual estimation of the light direction [9]. Aerial perspective, which is caused by the scattering effect along the reflected light from the given voxel to the viewpoint, produces depth cues for participating media [12]. We did not consider specular illumination, because it highlights artificial features that might be misinterpreted and ruin the visual cues for the local shape perception.

The scattering effect of the reflected light is not implemented in the multidirectional occlusion model [38], but we still can simulate the aerial perspective using the difference of luminance that comes from the scattering effects of the incident light. The cast shadow is also generated by the incident light, which is affected by the voxels along a light ray. Consequently, we classify the cast shadow and aerial perspective as *global effects*. In most perceptual experiments regarding the diffuse reflection and attached shadow [9], [19], the objects are opaque, the lighting is consistent, and the scattering effect is negligible. In these experiments, the diffuse reflection and attached

shadow are only affected by the diffuse ratio, which depends on gradient. Therefore, we classify the diffuse reflection and attached shadow as *local effects*. The key light produces both local and global lighting effects.

As for the fill light, a frequently employed measure of perceptibility is just-noticeable-difference [43] (also called Weber ratio), which is the minimal luminance change required for an observer to perceive a difference. The sensitivity of the human visual system to the luminance change is a function to the perceived luminance [13]. The lower the perceived luminance of a local region is, the poorer the luminance discrimination ability is [14]. According to the Phong shading model, the luminance is a product of the illuminance and diffuse ratio. The diffuse ratio is the primary source of the visual cues for local shapes, which is emphasized by the detail light. In order to separate the configuration of the fill light from that of the detail light, we estimate the perceptibility using illuminance instead of luminance when setting the fill light. The perceptibility estimated using illuminance measures the potential perceptibility before adding detail lights. For increasing the perceptibility, the fill light only produces global lighting effects and it does not affect cues for local shapes conveyed by the key light. The detail light is finally configured based on both the key light and fill light. It only produces local lighting effects to enhance the visual cues for local shapes.

The global impression relates to all the lights. Several observations [2], [33] state that the human visual system has a preferable assumption to believe that a scene is lit by a single light. Several lights with similar intensity yield lighting effects that are perceived by the visual system as contradictory (as in Fig. 1d). Anomalies in lighting directions are perceptually very salient in an image with regularity [31]. Consequently, our system uses only one key light. Fill lights and detail lights work as accessory lights. In the configuration of the accessory lights, the global impression is preserved by maintaining the visual estimation of the light direction.

4 AUTOMATIC LIGHTING DESIGN

Our lighting design algorithm is divided into three steps: the configuration of the key light, fill lights, and then detail lights. In each step, an objective function C is provided as a measure of the perception of 3D objects.

A perception of objects is stimulated by a rendered image, where each voxel in the volumetric data is represented by a pixel. To measure the contribution of a voxel to the rendered image, we first propose the computation of the perceived luminance $L(i)$ (defined in Section 3) being the multiplication of voxel i 's luminance (i.e., its diffuse reflection $diffuse(i)$) and its visibility $visibility(i)$ in the scene (1). The $visibility(i)$ is derived from the absorption component of the optical model for direct volume rendering [10]. It takes the influence of translucent material into account.

$$visibility(i) = visibility_{acc}(i) \times (1 - \exp(-\tau_i)), \\ L(i) = visibility(i) \times diffuse(i), \quad (1)$$

where τ_i is the extinction coefficient of voxel i . $visibility(i)$ is the multiplication of voxel i 's opacity (i.e., $1 - \exp(-\tau_i)$)

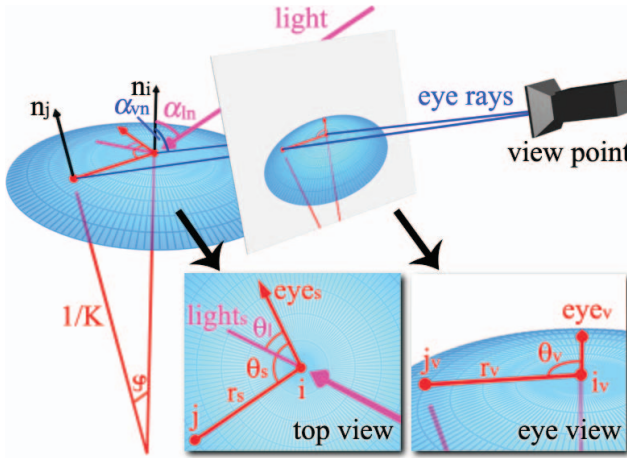


Fig. 3. Illustration of the relationship between the points (i_v and j_v) in the rendered image (the subfigure marked eye view) and voxels (i and j_v) on a local surface (shown in the subfigure marked top view; the top view is a view looking in the opposite direction of the surface normal n_i).

and its accumulated transparency (i.e., $visibility_{acc}(i) = \exp(-\sum \tau_{eye}(i))$, with $\tau_{eye}(i)$ representing the extinction coefficient of the voxels along the eye ray emitting from the viewpoint before arriving at voxel i). The diffuse reflection $diffuse(i)$ is the same as that in the Phong shading model ($diffuse(i) = Ill(i) \times ratio(i)$, with $Ill(i)$ being the illuminance at voxel i and $ratio(i)$ being the diffuse ratio).

However, the difference of $L(i)$ recognized by an observer is effected by the sensitivity of the human visual system (i.e., the just-noticeable-luminance-difference $\Delta L(i)$ mentioned in Section 3). The relationship between $\Delta L(i)$ and $L(i)$ is well studied in psychophysics [14]. We use (2) as an approximation, with $L(i) \in [1, 256]$

$$\log\left(\frac{\Delta L(i)}{L(i)}\right) = 1 - \frac{3}{8} \log L(i). \quad (2)$$

Based on $L(i)$ and $\Delta L(i)$, we propose a set of objective functions in the following sections to measure the perception of 3D objects. They are our major contribution. Our lighting design algorithm then automatically finds the light directions with the maximum value in the objective functions. The global impression is maintained by setting the accessory lights with proper intensities based on the strength of preserving the light direction estimated by the human visual system. Since only directional lights are employed, a spherical coordinate system reduces the search space from 3D to 2D for a single scene.

4.1 Key Light

We create an objective function for the key light (C_{key} in (3)). It contains the local shape perception (C_{local} in (4)) and the global perception, which includes the perception from shadows (C_{shadow} in (9)) and aerial perspective (C_{aerial} in (10)). The attached shadow is the special diffuse reflection with an obtuse angle between the surface normal and the light. It passively conveys the global impression when it is consistent with a cast shadow [9], [19]. Therefore, C_{shadow} is computed only from cast shadows. Cast shadows and aerial perspective are global effects, which result in the difference of illuminance. The local shape perception comes from

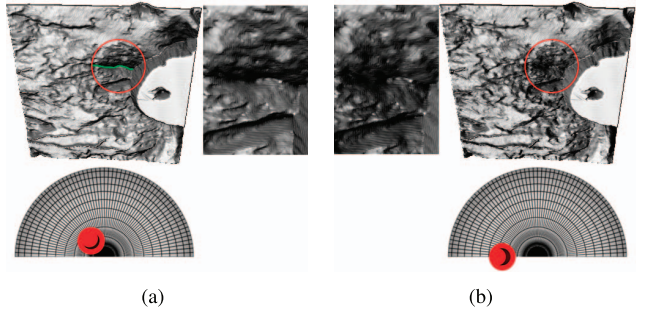


Fig. 4. Volume rendering of a voxelized crater using the key light with optimized (a) view-based gradient magnitude in our method, and (b) view-based discrete gradient magnitude. The black spherical grids represent the search space of the key light, with each cross point being a possible light direction. The red 3D arrows show the directions of the lights. In (a), the (green) concave region is clearly depicted in (a). In (b), the tiny curvature-based features are overstated and they disturb the visual cues for the shape of the concave region.

diffuse reflection, which comes from the diffuse ratio. Since the luminance (related to the brightness of a pixel in the rendered image) is a product of illuminance and the diffuse ratio, we use the multiplication of the local shape perception and the global perception as our objective function

$$C_{key} = C_{local} \times (C_{shadow} + C_{aerial}). \quad (3)$$

Local shape perception C_{local} represents the summary of local shapes perceived by an observer. The visual cues of a local shape are conveyed by the gradient magnitude ($g(i)$) of the perceived luminance in a rendered image. We divide $g(i)$ by the just-noticeable-luminance-difference $\Delta L(i)$ to measure the local shape perception

$$C_{local} = \sum \frac{g(i)}{\Delta L(i)}. \quad (4)$$

Equation (4) is our main equation for measuring the local shape perception. The gradient magnitude $g(i)$ is calculated using the perceived luminance $L(i)$ around voxel i in the rendered image (called eye view in Fig. 3).

It is possible to discretely compute $g(i)$ using $L(j)$ of i 's neighbor (assuming j in the eye view). However, this discrete $g(i)$ is affected by the curvature on a surface and emphasizes curvature-based features. It is shown in our user study (in Section 6) that the curvature-based method (Fig. 4b) provides inconsistent visual cues for local shapes (50 percent of observers think that the concave region is rendered deeper than the real shape with the other 50 percent thinking shallower).

Consequently, we compute $g(i)$ by using (5), with an assumption of uniformly distributed curvatures. Equation (5) is computed in the polar coordinate system with (r_v, θ_v) being the polar coordinate in the eye view (Fig. 3).

$$g(i) = \sqrt{\left(\frac{\partial L(i)}{\partial r_v}\right)^2 + \left(\frac{\partial L(i)}{r_v \times \partial \theta_v}\right)^2}. \quad (5)$$

The computation of $\partial L(i)$ requires to represent $L(j)$ (voxel j is a neighbor of voxel i) to be represented as a function of i . A surface having uniformly distributed curvatures is a spherical surface, and hence it is safe to assume that a local region is a plane and all the voxels on it

have the same visibility and the same illuminance (i.e., for any voxel j on this surface, $\text{visibility}(j) = \text{visibility}(i)$ and $\text{Ill}(j) = \text{Ill}(i)$). According to the equation of $L(j)$ and, in turn, the equation of $\text{diffuse}(j)$, $\text{ratio}(j)$ becomes the only component not related to i . As shown in the top view of Fig. 3, the projection of the light direction and the eye ray on the local surface are light_s and eye_s , respectively. Using i as origin and eye_s as polar axis, the position of any voxel j on the local surface is represented as $(r_s(j), \theta_s(j))$ in the polar coordinate system. light_s is represented as $\theta_l(i)$. $\text{ratio}(j)$ can be calculated as $\cos \varphi(j) \times \cos \alpha_{ln}(i) + \sin \varphi(j) \times \sin \alpha_{ln}(i) \times \cos(\theta_s(j) - \theta_l(i))$, where $\varphi(j)$ is the angle between normals at voxel i and j (i.e., n_i and n_j). $\alpha_{ln}(i)$ is the angle between the light and normal n_i . Since the curvatures are uniformly distributed, it is safe to assume that K_i is a constant in each local region. Then, $\sin \varphi(j) \approx r_s(j) \times K_i$ and $\text{ratio}(j)$ is represented as a function of $(r_s(j), \theta_s(j))$.

Finally, for the computation of $g(i)$ (which contains $\frac{\partial L(i)}{\partial r_v}$ and $\frac{\partial L(i)}{\partial \theta_v}$), we need to relate $(r_s(j), \theta_s(j))$ with $(r_v(j), \theta_v(j))$. As shown in the eye view of Fig. 3, voxel i is projected to i_v and the projection of eye_s is eye_v . Using i_v as the origin and eye_v as the polar axis, the projection of voxel j in the eye view (j_v) is represented as $(r_v(j), \theta_v(j))$. We have

$$r_s(j) = r_v(j) \times \sqrt{(\sin \theta_v(j))^2 + \left(\frac{\cos \theta_v(j)}{\cos \alpha_{vn}(i)} \right)^2}$$

and $\tan \theta_s(j) = \tan \theta_v(j) \times \cos \alpha_{vn}(i)$, where $\alpha_{vn}(i)$ is the angle between eye ray and n_i .

Combining the equations above, $g(i)$ is computed in (6).

$$w_l(i) = |\sin \alpha_{ln}(i)| \times \sqrt{(\sin \theta_l(i))^2 + \left(\frac{\cos \theta_l(i)}{\cos \alpha_{vn}(i)} \right)^2}, \quad (6)$$

$$g(i) = \text{visibility}(i) \times \text{Ill}(i) \times K_i \times w_l(i).$$

When the curvatures are uniformly distributed over all the objects, K_i is a constant. It will not affect the lighting design, hence we remove K_i from the equations and get C_{local} :

$$C_{local} = \sum_{i \in \text{view}} \frac{\text{visibility}(i) \times \text{Ill}(i) \times w_l(i)}{\Delta L(i)}. \quad (7)$$

Using the C_{local} , we obtain a more consistent result (Fig. 4a, with 75.8 percent selections of the user study showing that our approach enhances the visual cues for the local shape perception). Fig. 4a shows that it is necessary and possible to improve the visual cues for the local shape perception and to diminish the influence of the curvature-based features.

Shadows only involve cast shadows. A cast shadow carries the visual cues for the global shape perception of the object casting it (termed casting object) and the object on which it is cast (termed background object), as shown in Fig. 5. The visual cues for the global shape perception of these two types of objects are conveyed in different ways [23]. For the casting object, the visual cues help to identify it and to predict the light direction [9]. For the background object, the visual cues assist the observer in estimating its relative depth [23] (referred to as for depth perception in some literature). In addition, the relationship between casting and background objects also expresses their spatial arrangement [27]. The spatial arrangement is naturally conveyed so that it does not need an objective function.

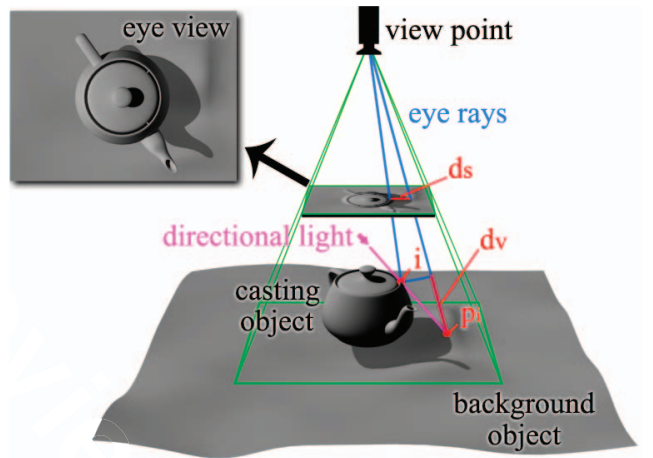


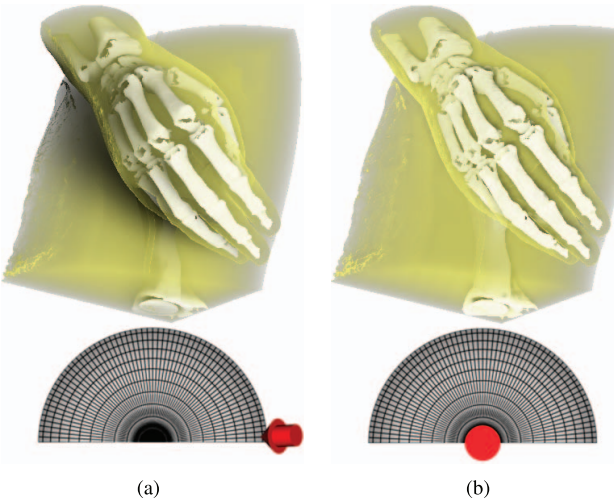
Fig. 5. Illustration of shadows. It shows the perceived shadow length d_s , perceived relative depth d_v , voxel i and the point on its shadow's contour (p_i). We use surface models for illustration, but our algorithm also works for translucent objects in volume data.

Therefore, for C_{shadow} , we only measure the global shape perception for the casting and background objects, and ignore the spatial arrangement. For the casting object, congruent cast shadow provides better visual cues and shortens the time for identifying accurate shapes [9]. The mathematical definition of congruence between two sets of points is that one set can be transformed into the other by an isometry, and isometry is defined as a distance-preserving map between two corresponding points. Based on the lighting model, the correspondence between the point (p_i) on a shadow's contour (i.e., a point in one set) and the voxel (i) casting it (i.e., a point in the other set), is naturally established (Fig. 5). The isometry is the map from i to p_i . In other words, the isometry maps the relative depth between a voxel and its shadow (i.e., the perceived relative depth d_v) to the perceived shadow length d_s . Therefore, the isometry represents the linear relationship between d_v and d_s . For the background object, the visual cues for the global shape perception are also conveyed by the linear relationship between the perceived relative depth d_v and the perceived shadow length d_s [27]. Consequently, the strength of the linear dependence between d_v and d_s describes the strength of visual cues for the global shape perception of both the casting and background object. However, in the rendering model with scattering effect, the contour of a shadow is blurred. We create a $w_{shadow}(i)$, which is the perceived contrast of voxel i , to represent the perceived possibility of a point to be on a shadow's contour, as shown

$$w_{shadow}(i) = \frac{\text{visibility}_{acc}(p_i) \times \text{contrast}(p_i)}{\Delta L(p_i)}. \quad (8)$$

$\text{contrast}(p_i)$ refers to the possibility of a point to be on a shadow's contour. Multiplying by $\text{visibility}_{acc}(p_i)$ measures the possibility after traveling through the volume data. It considers the influence of the translucent material. We divide the product by $\Delta L(p_i)$ to represents the possibility obtained by an observer.

In order to measure the strength of the linear dependence between d_v and d_s with w_{shadow} being the weight, we employ the weighted Pearson correlation coefficient ($\text{corr}(x, y; w)$). The $\text{corr}(x, y; w)$ is a tool for measuring the



(a)

(b)

Fig. 6. Rendered global effects of the Visible Woman's right hand (a) using the key light with the maximum global shape perception, and (b) using a single headlight. The translucent material is rendered in light yellow. The shadow in (a) depicts the shape of the woman's hand and the curve of the woman's body. It conveys the spatial arrangement between her hand and body.

strength of linear dependence between two variables x and y with a weight vector w [34]. Its value is $[-1, +1]$ and reaches ± 1 when the relationship is linear. We use its absolute value

$$C_{shadow} = |\text{corr}(d_s, d_v; w_{shadow})|. \quad (9)$$

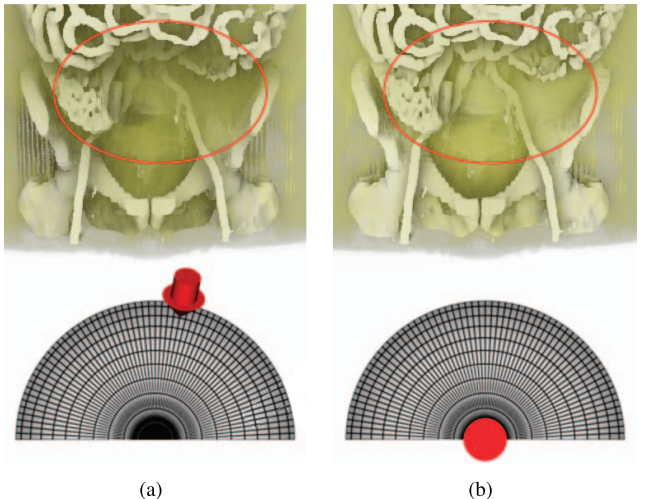
The result of using the key light with the maximum global shape perception is shown in Fig. 6. In the user study, 78.1 percent selections show that our method conveys accurate global shapes, meanwhile, 83.3 percent selections show that the object rendered with a single headlight looks flatter. Fig. 6 demonstrates that it is necessary and possible to improve the visual cues for the global shape perception by using the key light.

Aerial perspective is caused by the scattering effect and is represented as a decrease in luminance contrast. It conveys the visual cues for the depth perception of translucent structures. The luminance contrast decreases with the logarithm of distance [11], [30]. We compute the strength of logarithmic dependence between the luminance contrast decrease and the distance using the strength of linear dependence between the logarithmic luminance contrast decrease

$$(\log_{contrast}(i) = \log(contrast_v(i)) - \log(contrast_s(i)))$$

and the distance ($dep(i)$). The $contrast_s(i)$ represents the luminance contrast at voxel i and $contrast_v(i)$ refers to the luminance contrast of the rendered image at the corresponding position.

Nevertheless, in practice, a volumetric data set is always rendered into different materials, using different colors, transparencies, specularities, diffuse ratios, etc. Material identification itself remains a challenge. Existing psychophysical research is not sufficient for producing a sophisticated perception-based material identification algorithm. Therefore, we calculate the depth perception (C_{aerial}) with the assumption that the translucent material in a data set is



(a)

(b)

Fig. 7. Rendered global effects of a CT abdomen data set (a) using the key light with the maximum depth perception, and (b) using a single headlight. In the red ellipse, the cues for the depth of the (light yellow) translucent material are revealed in (a), while the structures in (b) look flat.

unique, and we create a weight $w_{aerial}(i)$ to represent the possibility of the voxels along an eye ray belonging to the same material. To quantify $w_{aerial}(i)$, we construct a material model to represent the material involved in volume rendering. Our material model contains two components: color and opacity. Because color and opacity are the parameters used by the human visual system for material differentiation [42], they are the major optical parameters employed in transfer function design. For the color component, a perceptually uniformly distributed color model, Lab is used. However, we ignore its luminance component, because the lightness constancy of the human visual system constrains the influence of luminance on the material perception [3]. Consequently, our material model is $(a, b, opacity)$. w_{aerial} is calculated using the reciprocal of the weighted variance of each voxel's normalized $(a, b, opacity)$ along an eye ray, with visibility being the weight.

We compute C_{aerial} using the weighted Pearson coefficient of the translucent material depth (i.e., the distance) and the logarithmic luminance contrast decrease, weighted by $w_{aerial}(i)$:

$$C_{aerial} = \text{corr}(dep, \log_{contrast}; w_{aerial}). \quad (10)$$

The rendering result of using the key light with the maximum depth perception is shown in Fig. 7. In our user study, 91.7 percent selections show that our method conveys better visual cues for the depth perception than a single headlight. Fig. 7 demonstrates that it is necessary and possible to improve the visual cues for the depth perception by using the key light.

4.2 Fill Light

Fill lights adjust the illuminance (i.e., global effects) to increase the perceptibility and preserve the global impression. Though the global impression is conveyed by both cast shadows and attached shadows, the attached shadow belongs to the local effects. Fill lights only affect the global impression conveyed by cast shadows. We use the strength of global impression preservation (S_{fill} in (12)) as a weight,

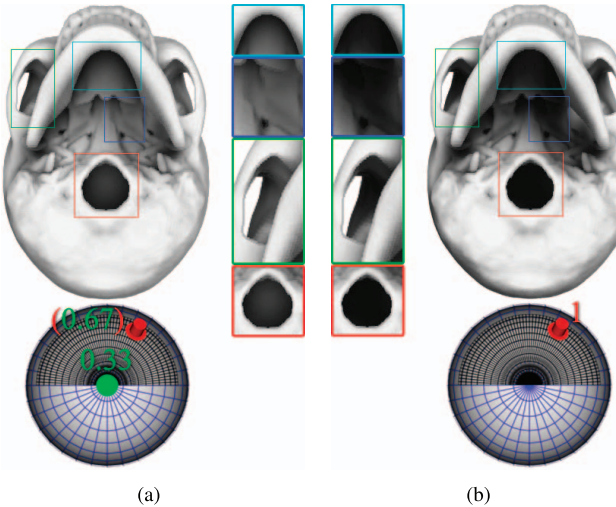


Fig. 8. Comparison of the global effects of a voxelized skull data set (a) with and (b) without fill lights. The blue 3D grid shows the search space of the fill lights, with each cross point representing a possible light direction. The green 3D arrow represents the direction of the fill light with its intensity marked. It is shown as a dot, because it points in the view direction. Fill lights fill the shadows and preserve the global impression.

and hence C_{fill} is the multiplication of S_{fill} and the perceptibility of the scene (P_{fill} in (13)), as shown

$$C_{fill} = S_{fill} \times P_{fill}. \quad (11)$$

S_{fill} is used to preserve the visual estimation of the light direction, which comes from the direction of the cast shadows. Therefore, we propose to use the strength of cast shadow preservation as S_{fill} . The scattering effect blurs the cast shadows and makes a shadow have different brightness. To preserve the brightness difference in a shadow, we use the strength of the linear dependence between the cast shadow of the key light Ill_{key} and that after adding fill lights Ill_{after}

$$S_{fill} = corr(Ill_{key}, Ill_{after}; visibility). \quad (12)$$

Ill_{after} is calculated using the weighted mean of illuminance of the key light and fill lights using their intensities as weights. Since the cast shadow belongs to the global effects where the illuminance is low, we compute S_{fill} within the scope of low illuminance voxels (illuminance < 0.2 in our experiments).

P_{fill} represents the total contrast that an observer can recognize in a scene. We compute it using the illuminance contrast ($contrast_{ill}$) dividing the just-noticeable illuminance difference ($\Delta Ill_{after}(i)$) of a scene. In a local region, the $\Delta Ill_{after}(i)$ is similar as the $\Delta L(i)$ in (2) with illuminance taking the place of luminance. To consider the $\Delta Ill_{after}(i)$ for a whole scene, we use the weighted mean of the reciprocal of the $\Delta Ill_{after}(i)$

$$P_{fill} = contrast_{ill} \times \frac{\sum \frac{visibility(i)}{\Delta Ill_{after}(i)}}{\sum visibility(i)}. \quad (13)$$

Using C_{fill} , fill lights are imported one by one. When the perceptibility increase becomes too small (< 0.001 in our experiments) or the global impression is almost destroyed ($S_{fill} < 0.4$), our algorithm will stop adding new fill lights. In most cases, our lighting system uses one fill light. As shown in Fig. 8, fill lights increase the perceptibility and preserve the global impression of the cast shadows.

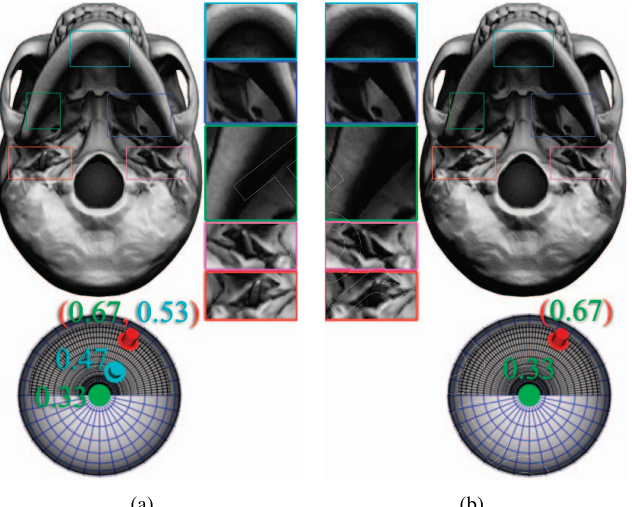


Fig. 9. Comparison of the rendered skull data set (a) with and (b) without detail lights. The search space for the detail lights is the same as that for the fill lights. The detail light is represented as a light blue 3D arrow. It enhances the visual cues for the local shape perception.

4.3 Detail Light

Detail lights produce local lighting effects to improve the visual cues for local shape perception. It only affects the global impression of attached shadows. We use the multiplication of the strength of global impression preservation (S_{detail} in (15)) and the local shape perception (P_{detail} in (16)) as the objective function of detail lights, as shown

$$C_{detail} = S_{detail} \times P_{detail}. \quad (14)$$

S_{detail} is similar to S_{fill} . We use the linear dependence between the attached shadows of the key light and attached shadows after adding detail lights as the S_{detail} :

$$S_{detail} = corr\left(\text{ratio}_{key}, \text{ratio}_{after}; visibility \times \frac{Ill}{\Delta Ill}\right), \quad (15)$$

where ratio_{after} is the weighted mean of diffuse ratios of the key light and detail lights using their intensities as weights. The weight ($visibility \times \frac{Ill}{\Delta Ill}$) takes the perceptibility into account. Since the attached shadow belongs to the diffuse reflection where the diffuse ratio is low, we compute S_{detail} within the scope of low diffuse ratio voxels ($\text{ratio} < 0.2$).

P_{detail} is calculated using the sum of perceived gradient magnitude after adding detail lights, which is similar to C_{local} :

$$P_{detail} = \sum_{i \in view} \frac{visibility(i) \times Ill(i) \times w_{detail}(i)}{\Delta L(i)}, \quad (16)$$

where

$$w_{detail} = \frac{\sqrt{\left(\sum (I \sin \alpha_{ln} \sin \theta_l)\right)^2 + \left(\sum \left(\frac{I \sin \alpha_{ln} \sin \theta_l}{\cos \alpha_{vn}}\right)\right)^2}}{\sum I}$$

with I being the intensity of each light.

Detail lights are added into our lighting system one by one. The stop condition is the same as that of the fill lights. In most cases, our lighting system imports up to three detail lights. The result of using detail lights is shown in Fig. 9. Detail lights improve the visual cues for local shape

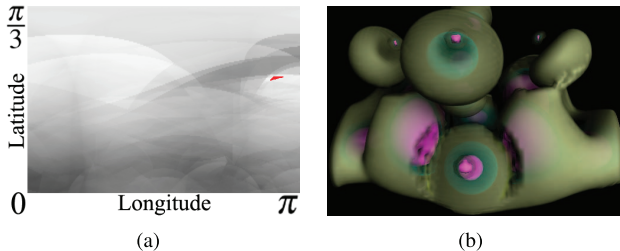


Fig. 10. (a) The values in the objective function of the key light with the Neghip data set and (b) the result using the key light in the direction with the global maximum value. The concave region with the global maximum value is marked red in (a).

perception and preserve the global impression of the attached shadows.

4.4 Lighting Design

The human visual system prefers light from the front and top [22]. The visual estimation of the light direction is decided by the key light. Therefore, the search space for the key light is a small region shown as the region covered by the black 3D grid in Fig. 9. Assuming the angle between the light and the view direction being latitude and the angle in the eye view being longitude, the search space of the key light covers the region of longitude between 0 to π and latitude between 0 to $\frac{\pi}{3}$. The search space for the accessory lights is the semisphere shown as the region covered by the blue 3D grid, which means longitude between $-\pi$ to π and latitude between 0 to $\frac{\pi}{2}$.

As shown in Fig. 10a, there exist numerous local maxima in the objective function of the key light. However, a gradient-based method can achieve the global maximum only if the initial light direction is inside the red region. Consequently, we use an exhaustive search to find the light directions. For accessory lights, our algorithm searches for the combination of intensity and direction. Our method simultaneously depicts the depth of the outer (yellow) object (in the right of Fig. 10b), the global (spherical) shapes of different layers, and the local shapes of the inner (magenta) object.

Our lighting design algorithm has the capability of ensuring smooth light movements for animations. The feeling of smooth movement captured by the human visual system is produced by the smooth change of the global impression [22], that, in turn, is conveyed by the key light in our lighting system. Therefore, we only constrain the movement of the key light. Accessory lights are configured on the fly.

The search space of the key light for a single frame of an animation is in 2D (Fig. 10a). The search space for a

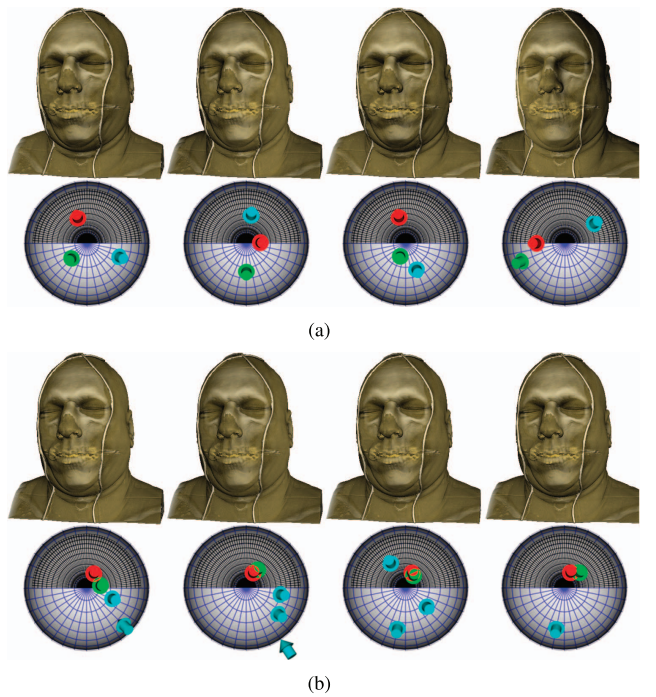


Fig. 12. Rendering of four continuous frames in the middle of a predesigned animation of the visible man's head using our method (a) without and (b) with constraining the key light movement. (b) Shows stable global impression changes across frames.

predesigned animation is in 3D, with each slice being the search space of a frame (Fig. 11). Finding a light path is the same as finding a line (the red line in Fig. 11) across all the slices. We obtain C1 continuous light movement by constraining the speed of the light between two adjacent points on this line. In our method, C2 continuity is also feasible. The selected line has the maximum sum of values in the objective functions of all the frames to guarantee that the maximum perception is obtained from the light path. This step is done by using dynamic programming. The results are shown in Fig. 12. When configuring the lights for each single frame separately, the lights jump between frames (as shown in Fig. 12a). After constraining the movement of the key light (Fig. 12b), the change of the global impression becomes stable.

5 SIMPLIFICATION AND IMPLEMENTATION

The exhaustive search in our algorithm is done in parallel, but an image needs to be rendered for each light direction. There is no graphics card with enough memory to accomplish this. Consequently, we propose a simplification for fast lighting design, in case speed is required for the given application. To achieve our goal, we approximate the shadows and change the way of computing the perception. The simplification is only used in the step of lighting design. With the simplification, our algorithm achieves interactive frame rates on a single GPU.

5.1 Shadow Approximation

Because of the scattering effect in translucent material, the boundaries of the cast shadows are blurred. It is possible to approximate the shadow from any given light direction

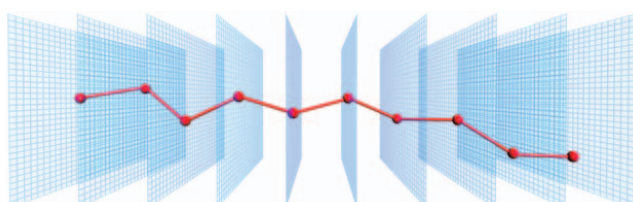


Fig. 11. The 3D search space for a predesigned animation. The red line represents the movements of the key light. Each slice is the 2D search space of a single frame.

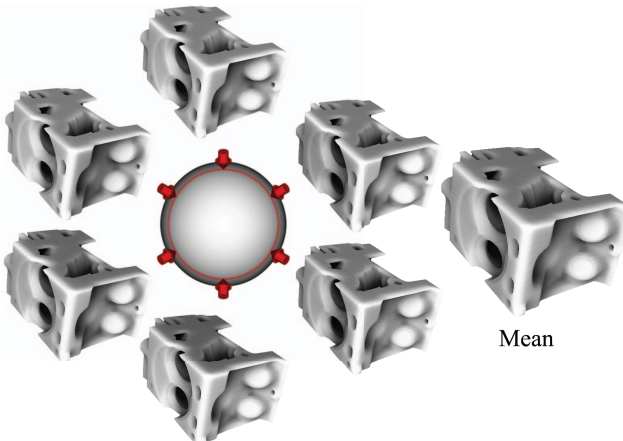


Fig. 13. The rendered engines lit from six directions with the same latitude ($\frac{\pi}{3}$). The rendered image lit by the mean global effects of the six directions is shown on the right.

using a linear interpolation of the shadows from fixed directions. We use $\frac{\pi}{3}$ as the aperture (the angle of scattering). When the angle between the light and the view direction (i.e., latitude) reaches $\frac{\pi}{3}$, the scattered light becomes parallel to the eye view. In this case, the rendered images using the light with different longitudes are similar, as shown in Fig. 13. The shadows stay consistent when the latitude is between $\frac{\pi}{3}$ and $\frac{\pi}{2}$.

Consequently, we use eight fixed directions (one with latitude being 0, six with latitude being $\frac{\pi}{6}$, and one being the mean, i.e., the mean of the six having $\frac{\pi}{3}$ as latitude in Fig. 13), as shown in Fig. 14, to approximate the global effects of any direction in the semispherical search space. The direction (marked 4) on the bottom of Fig. 14 is only used by accessory lights. We compute view aligned light volumes [36] from the eight directions and save them into two textures of type float4 in CUDA. In this way, we can fetch the eight global effects with only two operations. The global effects of the light at a given direction are calculated using a bilinear interpolation based on its direction. Using this method, there is no need to compute the global effects for all the light directions, only eight are calculated instead. The rendered

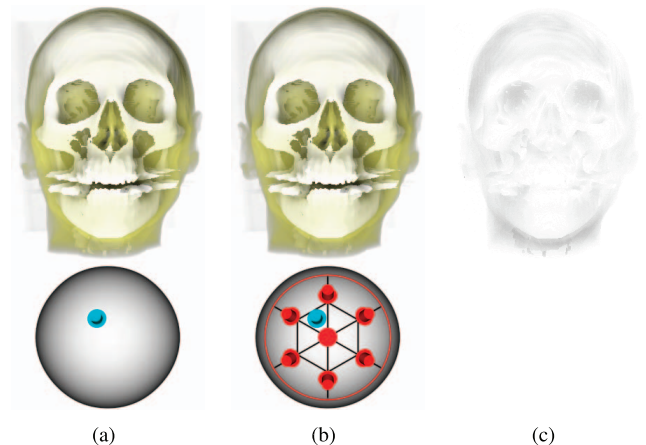


Fig. 15. The rendered global effects of a CT head using (a) accurate light direction, and (b) approximated global effects. (c) Shows five times the absolute difference.

result of the approximated shadows is visually similar to the result of using accurate light direction (Fig. 15).

5.2 Perception Computation

The computation of the perception obtained from diffuse reflection needs to traverse all the voxels in a given scene. It requires rendering the scenes with all the possible light directions. We modify it from traversing the voxels into visiting the entries in a normal table. The normal table is in 2D with a spherical coordinate system. Each entry in it represents a set of voxels having similar normals. This normal table is constructed by rendering the scene once, regardless of the light direction. The perception from diffuse reflection can then be efficiently calculated using it. As for the perception from the shadows and aerial perspective, the objective functions are related to the global effects. The global effects of the light at any direction in the search space are approximated by that of the eight directions. Therefore, only a depth buffer and 13 rendered scenes (6 for latitude $\frac{\pi}{3}$) are necessary for measuring the perception for all the light directions. In addition, because of using a view aligned light volume, the 13 rendered scenes are rendered in one pass. The lights configured using our simplified algorithm are not exactly the same as that using the accurate version, but the rendering results are visually identical, as shown in Fig. 16.

5.3 Parameter Selection

We have performed experiments to determine the parameters, including the weights of the objective functions, the sampling scheme, sampling rates of the key light and accessory lights, as well as the resolutions of the depth buffer, light volume, and normal table. We first determined the range of the parameters according to the memory limitation and speed. We then rendered the data sets with different shapes and recorded the running time of our simplified algorithm. The parameters were determined based on a visual evaluation and the running time. Further information is provided in Appendix A, which can be found on the Computer Society Digital Library at <http://doi.ieeecomputersociety.org/10.1109/TVCG.2012.91>.

Weights of objectives. We modified (3) to $C_{key} = C_{local} \times (\alpha \times C_{shadow} + (1 - \alpha) \times C_{aerial})$. We performed experiments

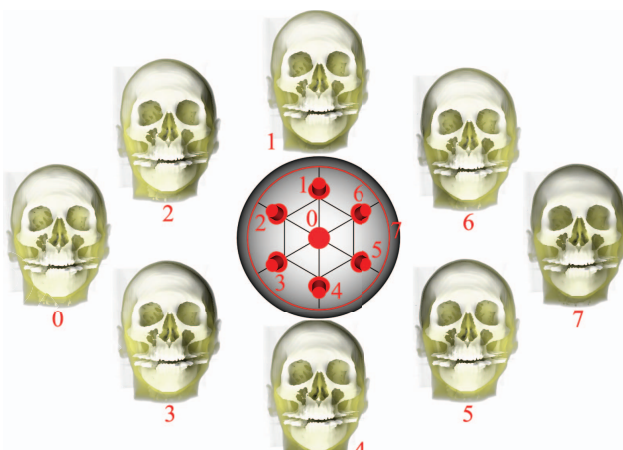


Fig. 14. The eight light directions (red 3D arrows) and corresponding rendered global effects on the CT head. The direction marked 7 is independent on longitude and is shown as a red circle.

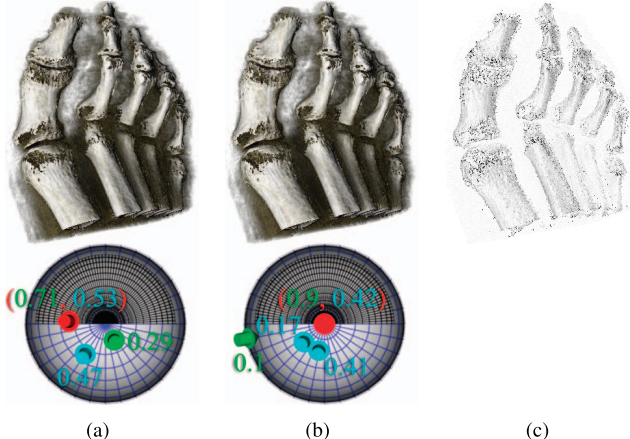


Fig. 16. Volume rendering of a CT foot data set using (a) the accurate lighting design algorithm, and (b) the simplified algorithm. (c) Shows five times the absolute difference.

on different data sets, with α varying from 0 to 1. Based on a visual evaluation, we decided to use 0.5 as a balance between the perception from shadows and aerial perspective.

Sampling scheme. We performed experiments using different sampling schemes, including the one used in our paper (shown as the blue 3D grids in Fig. 16) and an almost geodesic sphere. Since geodesic spheres typically have fewer sample points near the pole (latitude = 0), they always fail to ensure a global maximum when the global maximum is near the pole. Therefore, we decided to use the one shown as the blue 3D grids in Fig. 16 as our sampling scheme.

Sampling rates. We divided the longitude and latitude of a search space into segments, with each segment occupying $\frac{\pi}{2^n}$. We performed experiments with n varying from 4 to 8 to decide the sample rate for the key light, and from 4 to 7 for accessory lights. The influence of the sample rates on the rendered images is not very obvious, and hence we decided the sample rates mainly based on the running time. We determined to use 7 for the key light and 5 for the accessory lights.

Resolutions. We defined the resolutions as 2^n , with n varying from 5 to 8 for the depth buffer; 5 to 7 for the light volume and normal table. The resolution of the depth buffer relates to the amount of depicted local shapes, and hence we use 7. The resolution of the light volume does not affect the running time in its range, and it relates to visual cues for the depth perception, thus we use 7. As for the normal table, the rendered results of $n = 6$ and $n = 7$ are

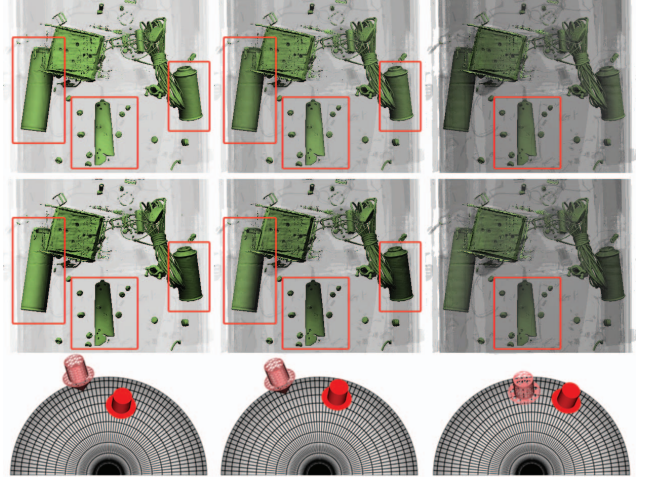


Fig. 17. Comparison between the volume renderings of a CT scanned backpack (top row) with and (middle row) without considering translucent structures. The solid red arrows in the bottom row show the direction of the key light with considering translucent structures, while transparent arrows are the direction without considering translucent structures. The opacities of the outer layers from left to right are 0.005, 0.01, and 0.02, respectively. The most different objects are marked with red rectangle frames.

similar, but the running time of $n = 7$ is dramatically high, therefore, we use 6.

6 RESULTS

Our method works for both surface and volumetric data sets. It considers the influence of translucent structures. As shown in Fig. 17, when considering the translucent layer, the light direction smoothly moves along the change of the outer layer's opacity. It provides visually consistent global effects for the inner structures. Without considering the translucent material, the light direction widely changes, and the global effects of the inner structures are inconsistent.

Our simplified lighting design method achieves interactive frame rates. The times for rendering a single scene using different data sets are recorded in Table 1. The light configuration time of the key light, fill lights, and detail lights are recorded separately. The time of the accurate and the simplified algorithms are written together with “/” as a separation mark. The numbers in the parentheses show the number of accessory lights. All the records are obtained on a desktop with eight 2.4 GHz CPU cores and six GB memory. The resolution of the rendered image is 512 by 512. The graphics card is NVIDIA GeForce GTX 480. Both the accurate

TABLE 1
Performance of Our Algorithm with Different Data Sets

Data type	Resolution	Total Time	Key Light	Fill Lights	Detail Lights	Rendering
Visible Man's head	512 × 512 × 512	429s / 363ms	161s / 78ms	96s(1) / 94ms(1)	171s(1) / 78ms(3)	111ms
Visible Woman's right hand	256 × 256 × 256	270s / 349ms	103s / 47ms	63s(1) / 109ms(1)	100s(1) / 141ms(8)	60ms
CT head	256 × 256 × 256	292s / 503ms	115s / 78ms	65s(1) / 109ms(1)	111s(1) / 265ms(15)	58ms
CT abdomen	256 × 256 × 64	251s / 299ms	97s / 62ms	56s(1) / 78ms(1)	97s(1) / 110ms(5)	61ms
CT foot	256 × 256 × 265	276s / 316ms	95s / 78ms	75s(1) / 94ms(1)	104s(1) / 93ms(5)	54ms
Voxelized crater	256 × 256 × 256	127s / 197ms	49s / 31ms	39s(1) / 47ms(1)	37s(1) / 78ms(4)	23ms
Mesh skull	256 × 256 × 256	131s / 168ms	49s / 47ms	43s(1) / 78ms(1)	39s(1) / 31ms(1)	24ms
Mesh pelvis	256 × 256 × 256	170s / 206ms	58s / 47ms	53s(1) / 93ms(1)	57s(1) / 31ms(1)	36ms

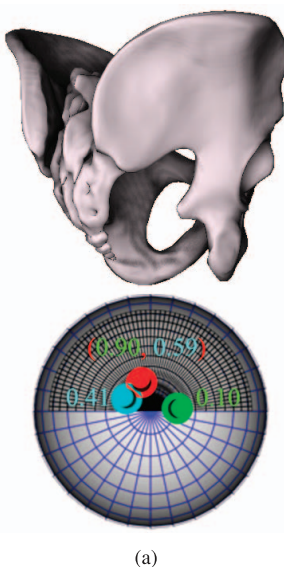


Fig. 18. Comparison between (a) our method, and (b) the algorithm of Lee et al. [24] (courtesy of their paper). Our method enhances the visual cues for the local shape perception and conveys accurate global shapes.

and simplified algorithms are running on the GPU. Table 1 shows that the total time of the accurate algorithm relates to the resolution and the complexity of a data set. The simple and opaque data sets, such as the voxelized crater and mesh data, are faster than other complex and translucent data sets. The low resolution data set CT abdomen is fast and the largest data set, the visible man's head, is the slowest. The time of the simplified algorithm depends more on the number of accessory lights and the complexity of a data set. The one with 15 detail lights (CT head) is the slowest and the simple data sets are fast. Our simplified algorithm is 500 to 1,000 times faster than the accurate one. The results of our method show advantages in conveying shape and depth perception when compared with the ones using former algorithms (Figs. 18 and 19).

We have conducted a user study to evaluate our lighting design method. We first set up a room with controlled ambient lighting conditions, where no overhead light or sunlight produces reflections and glare on the monitor. We then set the color space of the monitor to Adobe RGB, which contains a sufficient gamut for most output needs, while having only a slightly larger gamut than our monitor can display. We calibrated our monitor using a professional color calibration system, Spyder3. We changed the color temperature to 6,500 K and Gamma to 2.2. This setting is usually the best for working with Adobe RGB. Finally, we changed the background to a solid gray medium, which is the best for image review. All the above settings are summarized by Alsheimer and Hughes [5] for professional photographers.

In the user study, we divided our data sets into four groups based on their properties. The first group is about visual cues for single perception (Figs. 4, 6, and 7); the second includes opaque objects (mesh brain, CT scanned engine, and mesh skull); the third is translucent objects (CT scanned backpack, engine, and visible man's head); and the fourth compares our approach with previous methods (Figs. 18 and 19). The data sets in the second and third groups are with

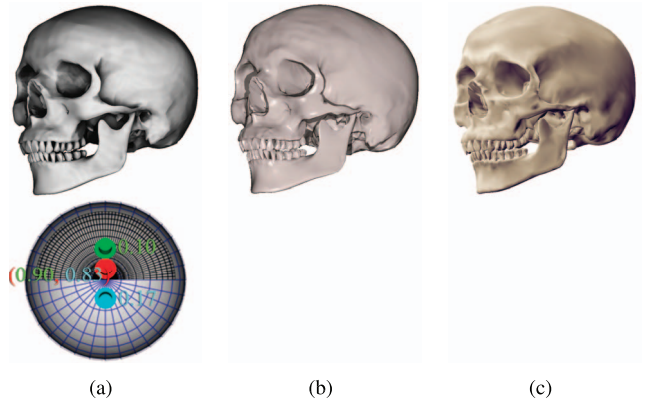


Fig. 19. Comparison between (a) our method, (b) the algorithm of Lee et al. [24] (courtesy of their paper), and (c) the algorithm of Rusinkiewicz et al. [35] (courtesy of their paper). Our method enhances the visual cues for local and global shapes.

different shapes: spherical shape (mesh skull and visible man's head), cubic shape (engine), complex local shape (mesh brain), and complex translucent material (backpack). In these two groups, our method is compared with a single headlight (the most common method in volume rendering), four consistent lights (a method that emphasizes local details), and the butterfly lighting method (a photographic method that emphasizes shapes). The observers include 6 visualization experts and 10 laymen.

We first produced a general user study, where we asked the observers to choose from the rendered images of the second and third groups the method that best represents the shape and depth perception. All the observers liked our approach and the visualization experts state that they do not like the shadows of the butterfly method. We then asked the observers to select their preferred light configuration in the fourth group. All the observers preferred our lighting results. They stated that our results provide more details and convey better global shapes. Finally, we asked the visualization experts to select the method most suitable for visualization applications. Eighty-three percent of them appreciate ours, with only one preferring a single headlight. He thought that a single headlight produces fewer shadows, but he admitted that our method conveys better visual cues for the shape and depth perception.

Two months after the general user study, when the observers have almost forgotten the images, we did a more detailed user study. In this user study, we asked the visualization experts to finish a series of tasks based on the visual cues for the perception of local shape, global shape, relative depth, and absolute depth, respectively. For each comparison, we extracted the surface of the object, and manually edited the surface to produce three surfaces with the testing features (i.e., the local shape, global shape or depth) on one of the surfaces being compacted, on one being accurate and on one being exaggerated. Each surface was rendered into three still images from three viewpoints lit by a single headlight. As shown in Fig. 20a, the concave region was modified shallow (compacted) in the top row and deep (exaggerated) in the bottom row for the study of local shapes. Similarly, we edited the extracted surfaces for the study of the global shape and absolute depth. As for the

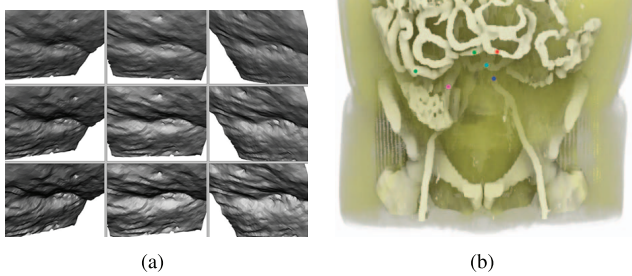


Fig. 20. Examples of our user study of the visual cues for the perception of (a) local shapes and (b) relative depth of the CT abdomen data set.

TABLE 2
Detailed User Study of the Local Shape Perception

Percentage	O	S	F	B	L	R
Compacted	15.2%	22.2%	21.9%	28.1%	25.0%	0.0%
Accurate	9.1%	30.6%	21.9%	15.6%	12.5%	100.0%
Exaggerated	75.8%	47.2%	56.3%	56.3%	62.5%	0.0%

study of the relative depth, we added colored dots (having the same size) in the rendered images, as shown in Fig. 20b.

The data sets were shown to the observers in a random order to avoid bias. The observers did not know which image was rendered using which method. In the study of the local shape perception, global shape perception, and depth perception, we first asked the observers to view the three surfaces (Fig. 20a) and required them to understand the difference of the surfaces before they saw the testing image. Then, we showed them the testing image and asked them to select a surface that was the most similar to the testing image. Additionally, in the study of local shapes, we circled the testing feature in the testing image. In the study of the relative depth, we asked observers to sort the dots (Fig. 20b) against the distance from the observer to the dots. We recorded the time an observer used in each test.

For different data sets we tested visual cues for different perception. In the first group, we tested the visual cues for the local and global shape perception, together with relative and absolute depth perception. In the second group, we tested the cues for the local and global shape perception. In the third group, the translucent objects are divided into two layers. For the outer layer, we tested the cues for the local and global shape perception. For the inner layer, we tested the cues for the local shape perception, and relative and absolute depth perception. In the fourth group, we tested the cues for the local and global shape perception, with relative depth perception. We did not test the cues for the absolute depth perception of the translucent material for the second and fourth groups, because they are opaque objects.

The result of our detailed user study are recorded in Tables 2, 3, 4, and 5. In these tables, "O" refers to our method, "S" is a single headlight, "F" is four consistent light, "B" is the butterfly method, "L" is the method of Lee et al. [24], and "R" is the method of Rusinkiewicz et al. [35]. Table 2 shows that our method conveys visual cues of exaggerated local shapes (75.8 percent). Although, the method of Rusinkiewicz et al. is said to exaggerate local shapes, it conveys the most accurate local shapes. Table 3 reveals that our method conveys the most accurate global shape (78.1 percent), the method of Rusinkiewicz et al. exaggerates the global shape,

TABLE 3
Detailed User Study of the Global Shape Perception

Percentage	O	S	F	B	L	R
Compacted	12.5%	83.3%	40.0%	35.0%	37.5%	0.0%
Accurate	78.1%	16.7%	40.0%	20.0%	12.5%	25.0%
Exaggerated	9.4%	0.0%	20.0%	45.0%	50.0%	75.0%

TABLE 4
Detailed User Study of the Relative Depth Perception

Percentage	O	S	F	B	L	R
Correctness	100.0%	100.0%	81.3%	87.5%	87.5%	75.0%

TABLE 5
Detailed User Study of the Absolute Depth Perception

Percentage	O	S	F	B	L	R
Compacted	8.3%	8.3%	12.5%	25.0%	N/A	N/A
Accurate	16.7%	66.7%	62.5%	12.5%	N/A	N/A
Exaggerated	75.0%	25.0%	25.0%	62.5%	N/A	N/A

the method of Lee et al. produces contradictions for different observers because it ignores the global impression. Table 4 represents the strength of visual cues for accurate relative depth. Our method and a single headlight are the best in this aspect. The method of Rusinkiewicz et al. is the worst (75.0 percent), since they use multiscale to optimize global perception. Table 5 displays that our approach exaggerates the absolute depth. It also shows that the visual cues for the depth perception of using a single headlight are accurate and that of the butterfly method are also exaggerated. In our detailed user study, the comparison results are similar for the objects with different shapes.

Fig. 21 displays the response time with standard deviation. A shorter response time means that the visual cues are easier for an observer to form the perception of the objects. Fig. 21 shows that our method dramatically improves the visual cues for the relative depth perception, since its response time is much shorter than that of others. For the perception of the local shape, global shape and depth, the compared methods show similar results, with ours being slightly better.

7 CONCLUSION AND DISCUSSION

In this paper, we have introduced a lighting system, which contains one key light and several accessory lights. Our lighting system conveys visual cues for local and global shape perception, as well as depth perception. We have also proposed a set of equations to measure the perception and have used an automatic lighting design algorithm to configure the lights. Our perception measurement considers the influence of translucent structures. It measures the local shape perception without the influence of curvature-based features. Our lighting design approach sets the lights in the directions where the perception of 3D objects is maximized. It configures accessory lights that preserve the global impression and solve the side effects of overillumination and shadows. It also ensures the impression of smooth light movements in predefined animations and achieves interactive frame rates with visually indistinguishable simplification. The contributions of this paper are our lighting system,

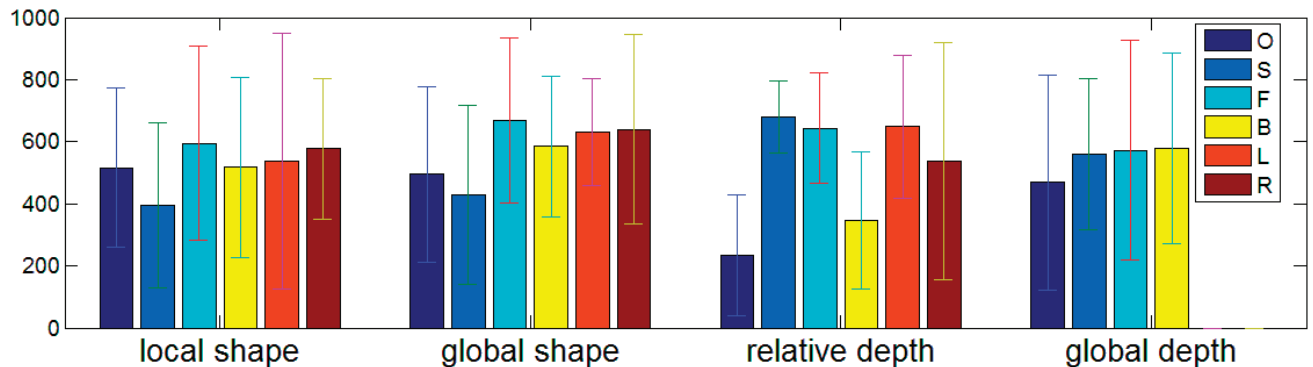


Fig. 21. The response time of the detailed user study with standard deviation. The colored bars show the mean response time, and the lines are the standard deviation. The unit of time is “ms.”

our perception measurements and our lighting design method with our visually indistinguishable simplification.

Nevertheless, our approach has its limitations. It does not support point lights and it limits the search spaces for acceleration. In the future, we plan to support point lights and to add a data driven sampling method that automatically changes the search space based on the scene. The assumption of a unique translucent material is another limitation of our method. It comes from the difficulty of material identification. In our future work, we want to imply material identification using color and opacity. We also intend to measure materials' density perception and configure the lights to convey it. Moreover, we want to consider assigning different weights to different shapes in our future work, so that our method can emphasize special shapes in a scene. In addition, our method depends on the transfer function design. For the data sets with unsteady gradients, such as an MRI data set, when using a poor transfer function, our lighting result is similar as using a single headlight. If the transfer function can provide more structural information, our lighting method is more useful. In the future, we plan to address this problem, probably by merging the transfer function design and lighting design steps.

ACKNOWLEDGMENTS

This paper has been supported by US National Science Foundation (NSF) grants IIS0916235 and CNS0959979 and NIH grant R01EB7530. The CT abdomen and chest data sets are courtesy of Stony Brook University Hospital and The Volume Library, respectively. All the other data sets are courtesy of volvis.org.

REFERENCES

- [1] A. Adams, *Basic Techniques of Photography*. Little Brown and Company, 1999.
- [2] E.H. Adelson and A.P. Pentland, *The Perception of Shading and Reflectance*. Cambridge Univ. Press, 1996.
- [3] E.H. Adelson, “Perception and Lightness Illusions,” *Perception*, vol. 3, no. 8, pp. 339-351, 2000.
- [4] J. Alton, *Painting with Light*. Univ. of California Press, 1995.
- [5] L. Alsheimer and B.O. Hughes, *Black and White in Photoshop CS3 and Photoshop Lightroom*. Focal Press, 2007.
- [6] A. Bousseau, E. Chapoulie, R. Ramamoorthi, and M. Agrawala, “Optimizing Environment Maps for Material Depiction,” *Computer Graphics Forum*, vol. 30, no. 4, pp. 1171-1180, 2011.
- [7] K. Berbaum, T. Bever, and C. Chung, “Light Source Position in the Perception of Object Shape,” *Perception*, vol. 12, no. 5, pp. 411-416, 1983.
- [8] S. Bergner, T. Möller, M. Tory, and M.S. Drew, “A Practical Approach to Spectral Volume Rendering,” *IEEE Trans. Visualization and Computer Graphics*, vol. 11, no. 2, pp. 207-216, Mar./Apr. 2005.
- [9] U. Castiello, “Implicit Processing of Shadows,” *Vision Research*, vol. 41, no. 18, pp. 2305-2309, 2001.
- [10] M.-Y. Chan, Y. Wu, W.-H. Mak, W. Chen, and H. Qu, “Perception-Based Transparency Optimization for Direct Volume Rendering,” *IEEE Trans. Visualization and Computer Graphics*, vol. 15, no. 6, pp. 1283-1290, Nov./Dec. 2009.
- [11] J.E. Cutting and P.M. Vishton, “Perceiving Layout and Knowing Distances: The Integration, Relative Potency and Contextual Use of Different Information about Depth,” *Perception of Space and Motion*, vol. 5, pp. 69-117, 1995.
- [12] W. Gerbino, C.I. Stultiens, J.M. Troost, and C.M. de Weert, “Transparent Layer Constancy,” *J. Experimental Psychology: Human Perception and Performance*, vol. 16, no. 1, pp. 3-20, 1990.
- [13] R.C. Gonzalez and P. Wintz, *Digital Image Processing*. Addison-Wesley, 1987.
- [14] R.C. Gonzalez and R.E. Woods, *Digital Image Processing*. Prentice Hall, Inc., 2001.
- [15] A. Gooch, B. Gooch, P. Shirley, and E. Cohen, “A Non-Photorealistic Lighting Model for Automatic Technical Illustration,” *ACM Trans. Graphics*, vol. 32, pp. 447-452, 1998.
- [16] S. Gumhold, “Maximum Entropy Light Source Placement,” *Proc. IEEE Conf. Visualization*, pp. 275-282, 2002.
- [17] M. Halle and J. Meng, “LightKit: A Lighting System for Effective Visualization,” *Proc. IEEE 14th Conf. Visualization*, pp. 363-370, 2003.
- [18] I. Iii, A.C. Costa, F. Nunes, and F. Iii, “Lighting Design: A Goal Based Approach Using Optimization,” *Proc. Conf. Rendering Techniques*, pp. 317-328, 1999.
- [19] A. Johnston and P.J. Passmore, “Shape from Shading. I: Surface Curvature and Orientation,” *Perception*, vol. 23, no. 2, pp. 169-189, 1994.
- [20] J. Kahrs, S. Calahan, D. Carson, and S. Poster, “Pixel Cinematography: A Lighting Approach for Computer Graphics,” *Siggraph Tutorials*, 1996.
- [21] A.A. Apodaca and L. Gritz, *Advanced RenderMan: Creating CGI for Motion Pictures*. Morgan Kaufmann, 2000.
- [22] D.A. Kleffner and V.S. Ramachandran, “On the Perception of Shape from Shading,” *Perception and Psychophysics*, vol. 52, no. 1, pp. 18-36, 1992.
- [23] D. Knill, P. Mamassian, and D. Kersten, “Geometry of Shadows,” *J. Optical Soc. of Am.*, vol. 14, no. 12, pp. 3216-3232, 1997.
- [24] C.H. Lee, X. Hao, and A. Varshney, “Geometry-Dependent Lighting,” *IEEE Trans. Visualization and Computer Graphics*, vol. 12, no. 2, pp. 197-207, Mar. 2006.
- [25] M. Levoy, “Display of Surfaces from Volume Data,” *IEEE Computer Graphics and Applications*, vol. 8, no. 3, pp. 29-37, May 1988.
- [26] B. London and J. Upton, *Photography*. Addison-Wesley, 1997.
- [27] P. Mamassian, D.C. Knill, and D. Kersten, “The Perception of Cast Shadows,” *Trends in Cognitive Sciences*, vol. 2, no. 8, pp. 288-295, Aug. 1998.

- [28] J. Marks, B. Andelman, P.A. Beardsley, W. Freeman, S. Gibson, J. Hodgins, T. Kang, B. Mirtich, H.P. Fister, W. Ruml, K. Ryall, J. Seims, and S. Shieber, "Design Galleries: A General Approach to Setting Parameters for Computer Graphics and Animation," *Proc. ACM SIGGRAPH*, pp. 389-400, 1997.
- [29] G. Millerson, *Lighting for Television and Film*. Focal Press, 1991.
- [30] S. Nagata, "Pictorial Communication in Virtual and Real Environments," *How to Reinforce Perception of Depth in Single Two-Dimensional Pictures*, S.R. Ellis, M.K. Kaiser, and A.C. Grunwald, eds., pp. 527-545, Taylor and Francis, Inc., 1991.
- [31] Y. Ostrovsky, P. Cavanagh, and P. Sinha, "Perceiving Illumination Inconsistencies in Scenes," *Perception*, vol. 34, no. 11, pp. 1301-1314, 2005.
- [32] F. Pellacini, P. Tole, and D.P. Greenberg, "A User Interface for Interactive Cinematic Shadow Design," *ACM Trans. Graphics*, vol. 21, no. 3, pp. 563-566, July 2002.
- [33] V.S. Ramachandran, "Perception of Shape from Shading," *Nature*, vol. 331, no. 6152, pp. 163-166, 1988.
- [34] J.L. Rodgers and W.A. Nicewander, "Thirteen Ways to Look at the Correlation Coefficient," *The Am. Statistician*, vol. 42, no. 1, pp. 59-66, Feb. 1988.
- [35] S. Rusinkiewicz, M. Burns, and D. DeCarlo, "Exaggerated Shading for Depicting Shape and Detail," *ACM Trans. Graphics*, vol. 25, no. 3, pp. 1199-1205, July 2006.
- [36] T. Ropinski, C. Döring, and C. Rezk-Salama, "Interactive Volumetric Lighting Simulating Scattering and Shadowing," *Proc. IEEE Pacific Visualization Symp.*, pp. 169-176, Mar. 2010.
- [37] R. Shacked and D. Lischinski, "Automatic Lighting Design Using a Perceptual Quality Metric," *Computer Graphics Forum*, vol. 20, no. 3, pp. 1-68, 2001.
- [38] V. Soltészová, D. Patel, S. Bruckner, and I. Viola, "A Multi-directional Occlusion Shading Model for Direct Volume Rendering," *Computer Graphics Forum*, vol. 29, no. 3, pp. 883-891, June 2010.
- [39] M.C. Sousa, F. Samavati, and M. Brunn, "Depicting Shape Features with Directional Strokes and Spotlighting," *Proc. Computer Graphics Int'l Conf.*, pp. 214-221, 2004.
- [40] R. Vergne, R. Paganowski, P. Barla, X. Granier, and C. Schlick, "Light Warping for Enhanced Surface Depiction," *ACM Trans. Graphics*, vol. 28, no. 3, pp. 1-8, 2009.
- [41] R. Vergne, R. Paganowski, P. Barla, X. Granier, and C. Schlick, "Radiance Scaling for Versatile Surface Enhancement," *Proc. Symp. Interactive 3D Graphics and Games (I3D)*, vol. 1, no. 212, pp. 143-150, 2010.
- [42] G. Wendt, F. Faul, V. Ekroll, and R. Mausfeld, "Disparity, Motion, and Color Information Improve Gloss Constancy Performance," *J. Vision*, vol. 10, no. 9, pp. 1-17, 2010.
- [43] S. Westland, H. Owens, V. Cheung, and I. Paterson-Stephens, "Model of Luminance Contrast-Sensitivity Function for Application to Image Assessment," *Color Research and Application*, vol. 31, no. 4, pp. 315-319, 2006.
- [44] S. Zhukov, A. Jones, and S. Kronin, "An Ambient Light Illumination Model," *Proc. Ninth Eurographics Workshop Rendering*, pp. 45-56, 1998.



Lei Wang received the BS degree in information science from the Beijing University of Posts and Telecommunications, China, in 2007. Currently, he is working toward the PhD degree in computer science at Stony Brook University, under the guidance of Arie Kaufman. His research interests include transfer function design, lighting design, volume rendering, registration, and medical imaging.



Arie E. Kaufman received the PhD degree in computer science from Ben-Gurion University, Israel, in 1977. Currently, he is a distinguished professor and chairman of the Computer Science Department, director of the Center of Visual Computing (CVC), and chief scientist of the Center of Excellence in Wireless and Information Technology (CEWIT) at Stony Brook University. He has conducted research for more than 40 years in visualization and graphics and their applications, has published more than 300 refereed papers, has presented more than 20 invited keynote talks, has been awarded/filed more than 40 patents, and has been PI/co-PI on more than 100 grants. He was the founding editor-in-chief of the *IEEE Transaction on Visualization and Computer Graphics (TVCG)*, 1995-1998. He is a fellow of IEEE, the IEEE Computer Society, and the ACM, and the recipient of the IEEE Visualization Career Award (2005).

▷ For more information on this or any other computing topic, please visit our Digital Library at www.computer.org/publications/dlib.